Surgical Oncology 31 (2019) 119–131

Contents lists available at ScienceDirect

Surgical Oncology

journal homepage: http://www.elsevier.com/locate/suronc

Multiphoton microscopy in surgical oncology- a systematic review and guide for clinical translatability

Tatjana Tamara König *, Jan Goedeke, Oliver J. Muensterer

Universitätsmedizin Mainz, Department of Pediatric Surgery, Mainz, Germany

ARTICLE INFO

Keywords:
Multiphoton imaging
Two-photon excited fluorescence
Second harmonic generation

ABSTRACT

Background: Multiphoton microscopy (MPM) facilitates three-dimensional, high-resolution functional imaging of unlabeled tissues in vivo and ex vivo. This systematic review discusses the diagnostic value, advantages and challenges in the practical use of MPM in surgical oncology.

Method and Findings: A Medline search was conducted in April 2019. Fifty-three original research papers investigating MPM compared to standard histology in human patients with solid tumors were identified. A qualitative synopsis and meta-analysis of 14 blinded studies was performed. Risk of bias and applicability were evaluated.

MPM can image fresh, frozen or fixed tissues up to a depth 1000 μm in the z-plane. Best results including functional imaging and virtual histochemistry are obtained by in vivo imaging or scanning fresh tissue immediately after excision. Two-photon excited fluorescence by natural fluorophores of the cytoplasm and second harmonic generation signals by fluorophores of the extracellular matrix can be scanned simultaneously, providing high resolution optical histochemistry comparable to standard histology. Functional parameters like fluorescence lifetime imaging or optical redox ratio provide additional objective information. A major concern is inability to visualize the nucleus. However, in a subpopulation analysis of 440 specimens, MPM yielded a sensitivity of 94%, specificity of 96% and accuracy of 95% for the detection of malignant tissue.

Conclusion: MPM is a promising emerging technique in surgical oncology. Ex vivo imaging has high sensitivity, specificity and accuracy for the detection of tumor cells. For broad clinical application in vivo, technical challenges need to be resolved.

1. Introduction

Multiphoton microscopy (MPM) was first described in 1990 by Denk et al. [1–3] (Fig. 1).The imaging technique is based mainly on the detection and combination of two signals: two-photon excited fluorescence (TPEF), and second harmonic generation (SHG), that are detected at specific emission wavelengths after laser excitation. MPM offers in vivo, real time, high resolution, functional visualization without need for contrast agents, tissue staining, or tissue processing [2,4] up to a tissue depth of several hundred microns [5]. Since 1990, a number of practical uses have been established in vitro and in vivo, in live animals, and even in humans [6]. Today, three-dimensional (multiphoton tomography, MPT), or even four-dimensional (multiphoton tomography with fluorescence lifetime imaging, MPT-FILM) signal detection is possible; either of unlabeled fresh [7], frozen [8] or formalin fixed [9] human tissues. In all cases, MPM has the potential of producing images of a comparable resolution to standard staining techniques, such as hematoxylin and eosin (HE), or others [8].

Natural fluorescence from endogenous fluorophores and second harmonic generation signals can be scanned simultaneously after excitation with only one wavelength [4]. Simultaneous absorption of two photons of lower energy leads to excitement of endogenous fluorophores without phototoxic tissue damage by high energy photons (Fig. 2). TPEF signals are mainly produced by excitation of cytoplasmatic and mitochondrial fluorophores, mainly reduced nicotinamide adenine dinucleotide (NADH) and oxidized flavin adenine dinucleotide (FAD) [4,7,8,10], but also by extracellular molecules like flavines [11] and collagen [12]. In contrast, SHG signal generally derives from collagen [12] of the extracellular matrix (Figs. 3 and 4). Longer (near infrared) excitation wavelengths enable a deeper tissue penetration [4,8] up to several hundred microns [5], or even 1000 μm in skin specimen [13]. In order to further differentiate between fluorescent structures, specific spectral ranges can be selected to create "virtual histochemistry" in fresh

* Corresponding author. Universitätsmedizin Mainz, Langenbeckstr 1, 55151, Mainz, Germany
E-mail address: tatjana.koenig@unimedizin-mainz.de (T.T. König).

https://doi.org/10.1016/j.suronc.2019.10.011
Received 25 June 2019; Received in revised form 2 October 2019; Accepted 13 October 2019
Available online 16 October 2019

Abbreviations

FAD	flavin adenine dinucleotide
FILM	fluorescence lifetime imaging
HE	hematoxylin/eosin
Λem	emission wavelength
Λex	excitation wavelength
MPM	multiphoton microscopy
MPT	multiphoton tomography
NADH	reduced nicotinamide adenine dinucleotide
NCR	nucleus-cell ratio
ORR	optical redox ratio
PBS	phosphate buffered saline
RCM	reflectance confocal microscopy
SHG	second harmonic generation
TPEF	two-photon-excited fluorescence

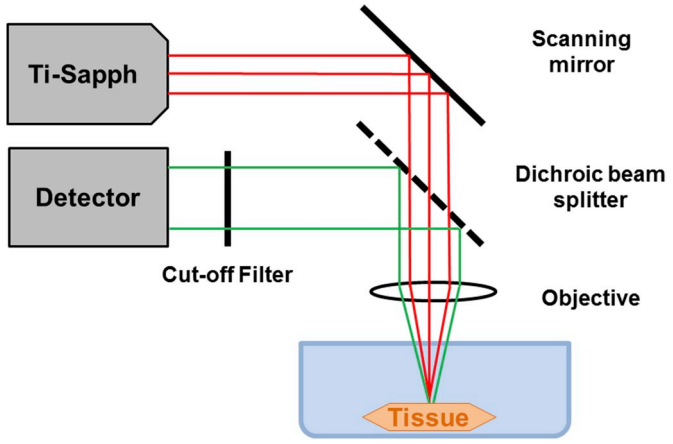

Fig. 1. Technical principles of MPM technology (Ti-Sapph = Ti-Sapphire femtosecond-pulsed Laser).

unlabeled tissue [14]. The spectral window of excitation wavelengths is limited by the phototoxicity of high energy photons, which can cause tissue damage, impaired reproduction capacity and apoptosis-like cell death [15].

Due to the relatively large dimensions of current MPM microscopes, use of the technology has mostly been limited to ex vivo imaging of histological specimen, which could theoretically be performed directly in the operating room under sterile conditions, for example to determine resection margins during surgical procedures [6,16]. Other limiting factors of current MPM technology are small scanning fields [17], and maximum scanning depth of 200 μm up to 800 μm, in certain circumstances up to 1000 μm, depending on the absorption and excitability of the tissue along with targeted magnification [6,8]. To date, in vivo multiphoton tomography (MPT) on humans has been used on skin lesions [18–20] and intraoperatively in a single patient with glioblastoma multiforme [6]. In these applications, the quality of MPM images was found to be comparable to ex vivo scans [6]. In the future, in vivo imaging may facilitate optical ad hoc biopsy combined with endoscopy or laparoscopy, "optical needle biopsy" [4], intraoperative real-time evaluation of resection margins [6,21] and nerve sparing surgery [22]. Even automated histopathological image analysis by machine ("deep") learning using artificial intelligence has been investigated [10]. Tissue evaluation using deep learning has been reported to yield sensitivity up to 95% and specificity as high as 97% for ovarian cancer cells [10] and accuracy over 90% for hepatocellular carcinoma [23]. This technology might give clinicians the opportunity of intraoperative MPM evaluation in absence of highly trained and specialized pathologists in the future.

The technology has some limitations. As mentioned, contemporary MPM hardware is quite spacious, and tissue penetration depth is limited. Current technical research focuses on development of smaller probes with longer wavelengths, that penetrate deeper into tissues and are less influenced by absorption and scattering of other molecules in the tissue (e.g. hemoglobin) [24]. Other general technical obstacles in the practical application of MPM are inhomogeneous signal intensity in varying depths, low signal-to-noise-ratio and blurring of cell boundaries, which increases in deeper tissue layers [2]. These challenges have been addressed by computer processing methods such as super pixel-based image segmentation and watershed [2]. Nevertheless, in regard of resolution, MPM offers unique high quality imaging on a submicron level, superior to other functional imaging techniques such as positron emission tomography, magnet resonance imaging or computed tomography [24].

In most cases, the established criteria for malignancy have traditionally been based on HE findings and include nuclear-cell ratio (NCR), cell and nuclear polymorphism, including chromatin condensation and mitosis, as well as apoptotic cells [25] (Figs. 3d and 4d). Crossing of suspect cells through the basal membrane is a sign of invasiveness [26]. In contrast to standard HE staining, cell nuclei [11] are not readily visualized directly by MPM, but are detected as an area with absence of TPEF/SHG signal [27,28], which is referred to as the "nuclear area" (Figs. 3 and 4). Therefore, to date, visualization of important cancer characteristics, like chromatin condensation, mitosis and apoptotic cell is still considered to be more accurate in HE stained specimen [25,28] (Figs. 3 and 4).

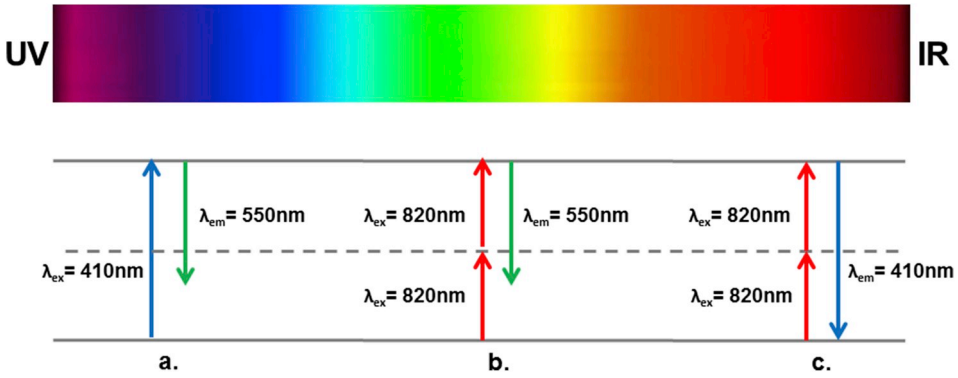

Fig. 2. Jablonski energy diagram for TPEF and SHG [81,82]. Photon energy of the excitation beam is higher than the emitted fluorescence. a. One Photon Excited Fluorescence: Excitation with one high energy photon. b. Two-Photon Excited Fluorescence: Excitement by two simultaneous photons with double with double wavelength c. Second Harmonic Generation Signal: $\lambda_{em} = \lambda_{ex}/2$. (UV = ultraviolet, IR = infrared,λ_{ex} = excitation wavelength, λ_{em} = emission wavelength).

Neoplasms can be detected and characterized by MPM depending on the ratio of cell organelles in the TPEF signal (e.g. NCR) [29]. Additional information can be obtained by analyzing collagen content and –distribution by its SHG signal, which is usually not easily detected in HE stained sections [11,27]. Basement membranes can be visualized by their SHG signal to determine cancer cell invasion [26]. Cell-to-cell communication mechanisms like tunneling nanotubes and their up-regulation in certain cancer types give another hint of tumor biology [30]. The optical redox ratio (ORR) as a measure of cell metabolism, can be defined by quantifying the tissue signal intensity of NADH and FAD at specific excitation wavelengths [11]. The ratio of free to protein bound NADH is an indirect measure of glycolysis and oxidative phosphorylation, thus reflecting the metabolic state of a cell [7]. Tumor cells show an elevated ORR compared to tumor tissues after chemotherapy or healthy tissues [11,31]. Fluorescence lifetime imaging (FLIM) is another additional MPM technique to discriminate further between different types of cells. Instead of detecting the fluorescence intensity, this technique quantifies the duration of fluorescence lifetime after laser excitation [17]. Further complementary imaging techniques are stimulated Raman scattering and coherent anti-Stokes Raman spectroscopy (CARS) [32]. These imaging techniques are based on vibrational microscopy and inherent specific scattering of tissue molecules (e.g. lipids) after laser excitation, facilitating intrinsic chemical mapping of tissues [32].

In basic research, three-photon excited fluorescence is a promising technique, providing improved optical sectioning and resolution compared to TPEF in a depth of up to 500 μm across the scull in a living mouse [33]. Excitation at longer wavelengths results in deeper tissue penetration, weaker scattering and therefore a better resolution in deeper tissue layers [33]. To our knowledge however, this technology has not been used in patients with solid tumors.

The objective of this systematic review is to determine the value of MPM imaging in surgical oncology, to identify specific tumor characteristics in MPM imaging, to compare to gold standard histopathology, and to discuss current clinical applications, latest advances and future possibilities, as well as the current limitations for MPM imaging for surgeons in the clinical setting.

2. Method

In April 2019, we performed a Medline search (see Appendix for search strategy) on studies regarding multiphoton microscopy in surgical oncology. Original research papers, comparing MPM imaging of unlabeled human tumor specimen (fresh, frozen, fixed) to standard histology were included. Exclusion criteria were animal studies, cell cultures or imaging after tissue labeling with fluorescent agents or dyes (PICOS Criteria, Table 1). A total of 549 abstracts were scanned. Review papers, case reports, animal and cell culture studies, and papers in languages other than English, German or French were excluded (Fig. 5). Papers meeting the inclusion criteria were assessed for eligibility by two separate reviewers. In case of disagreement, a third reviewer was consulted. A standardized, pre-piloted form was used to extract relevant data. Quality and applicability were assessed systematically by two separate investigators using the QUADAS-2 [34]. To assess quality of the included studies, sample selection strategy and qualification of investigators were taken into account. Further assessment criteria included weather MPM and standard histology were evaluated by the same investigator.

The group of blinded studies was analyzed separately as a subgroup. For blinded studies, sensitivity, specificity and accuracy were calculated using a 2x2 contingency table for each test with the numbers given in the studies. In cases where specimens were assessed by several independent investigators, the number of specimens was multiplied by the number of investigators blinded to standard histological diagnosis.

This review was registered at the PROSPERO registry

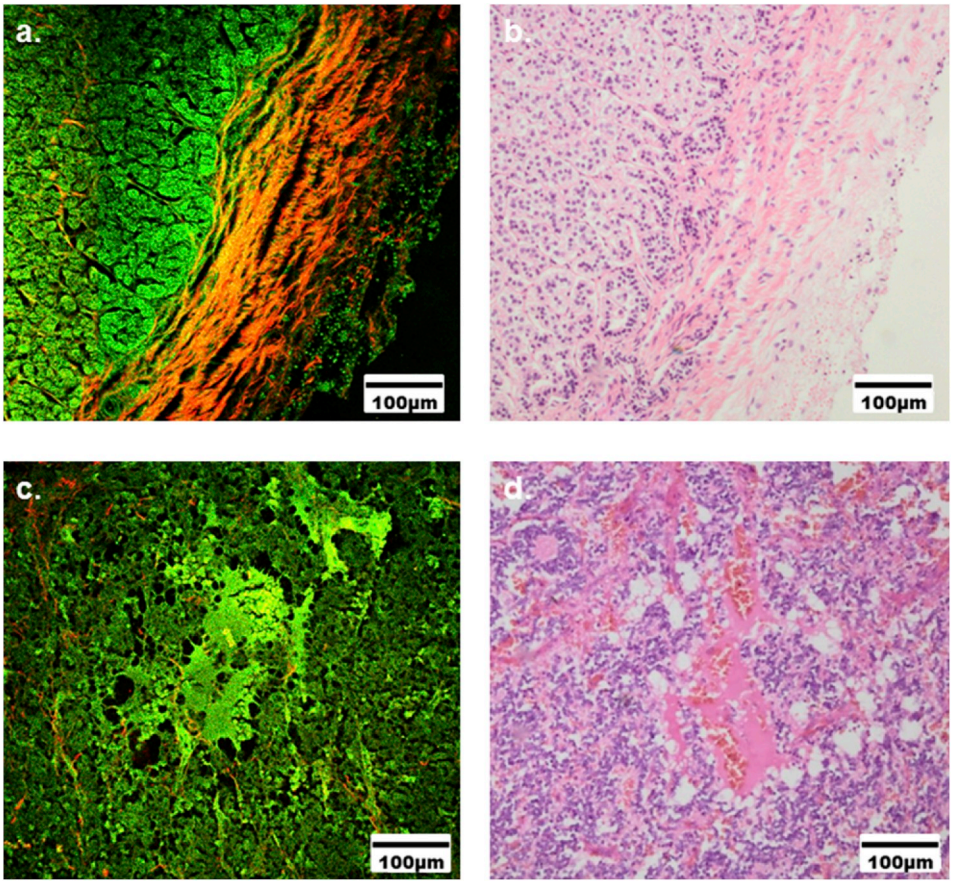

Fig. 3. a. Normal adrenal gland. Cells of the acini are clearly visible by their strong TPEF signal (color-coded green). Connective tissue of the capsule and in between individual acini is visualized by the SHG signal (clour-coded red) more clearly than in HE imaging (b.), c. MPM imgaing of a neuroblastoma shows loss of cell architecture, along with marked polymorphism of nuclear area and cells, d. These images shows the typical characteristics of neuroblastoma, including „small blue round cells“ and necrosis (corresponding HE image). (For interpretation of the references to color in this figure legend, the reader is referred to the Web version of this article.)

(CRD42019128424).

3. Results

A total of 188 studies were screened for eligibility, 53 original research articles published from 2007 through 2019 were selected for analysis by relevance. In each study, unlabeled human tissue was scanned with MPM for TPEF/SHG signals. In three studies [6,18,19], in vivo MPM imaging in human cancer patients was performed. In all other studies, TPEF/SHG signals were detected from fresh, frozen or fixed tissues after surgical or endoscopic resection (Table 1). MPM findings were validated by standard histological sections (HE) in 50 studies. In fourteen studies, the MPM examiner was blinded to the result of HE histology [12,28,35–46].

3.1. Types of tissues

The specific types of tissues scanned in the studies are shown in Table 2. The vast majority of studies (n = 22) were conducted in the fields of gastroenterology and general surgery (colorectal wall n = 8, gastric wall n = 8, esophageal wall n = 5, pancreas n = 2, liver n = 1), followed by gynecology (breast tissue n = 9, ovary n = 2) and urology (kidney n = 2, urothelium n = 2, prostate n = 2).

3.2. Tissue preparation

The imaging protocol was similar in most studies. In 26 studies, specimens were sectioned and consecutive sections were analyzed either by MPM or with the gold standard. In 19 studies, MPM scanning was performed and the same specimens were dyed with HE after MPM scanning. Only 13% of studies used a different protocol, half of those conducted in-vivo imaging.

Table 1
PICOS criteria.

PICOS criteria	inclusion criteria	exclusion criteria
participants	human tumor specimen (fresh, frozen or fixed)	animal studies studies on cell cultures, technical studies, healthy tissues
interventions	MPM imaging	
comparisons	standard histology, MPM imaging	
study design	blinded and unblinded original research studies	case reports, review papers

3.2.1. Fresh sections

Fresh tissue sections were scanned in 36 studies. Sections were cooled and scanned directly or after placement in phosphate buffered saline (PBS). The timeframe from resection to scanning was specified in 19 studies, mostly ranging from “immediately” to a 4 h interval. In only one study sections were kept on ice and scanned after 6–20 h [25]. Yan et al. showed that treatment with PBS is unnecessary to avoid drying and shrinkage, if tissue can be scanned without delay after excision [16]. One study compared scanning quality after different periods of time, showing a decrease of over-all fluorescence intensity of 23% after one, and 33% after 5 h in human brain tissue with marked alterations of the lipopigment signal in TPEF [47].

3.2.2. Frozen sections

Frozen sections were used in eleven studies, comprising breast tissue [11,43], esophageal or gastric mucosa [8,48,49], liver [45], lung [50], brain [51], and skin [52]. In some studies, freezing was performed for tissue sectioning in the freezing microtome [8]. In other studies, frozen tissues were obtained from a tissue bank [45]. One study indicates that specimens were defrosted for 10 min at room air before imaging [50]. In

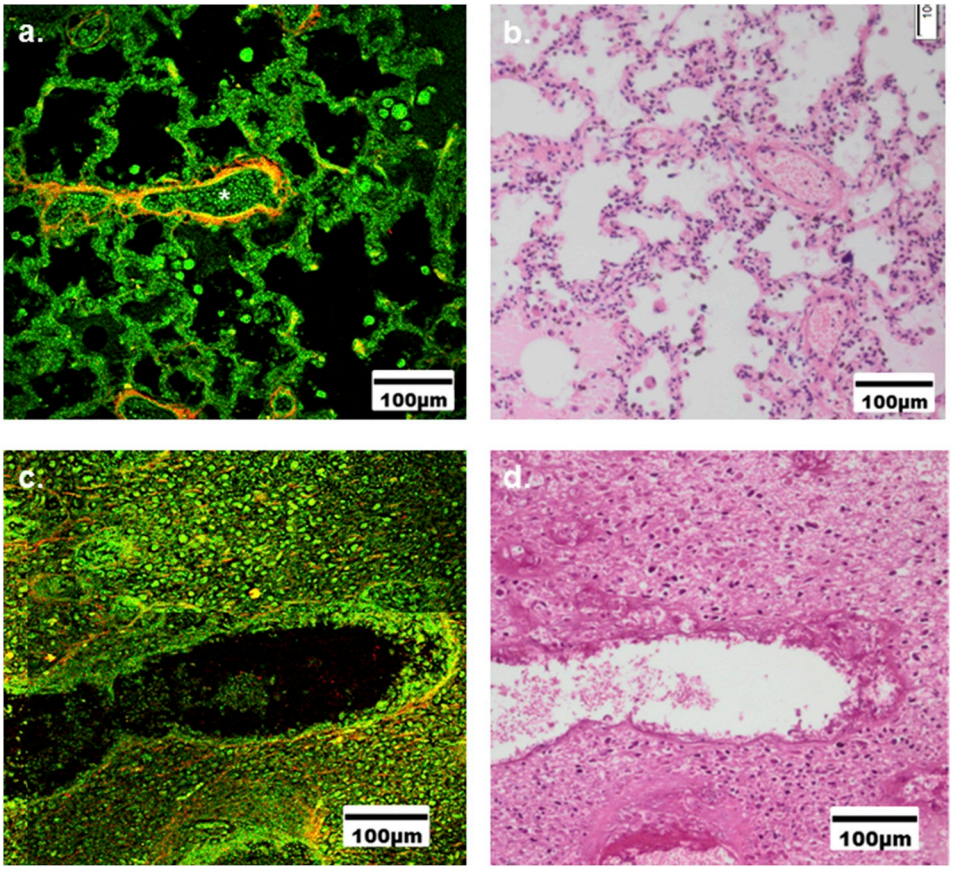

Fig. 4. a. Clear TPEF signal (color-coded green) of pneumocytes and intraalveolar cells in normal lung tissue. Central blood vessel (*) with SHG signal (color-coded red) of the vessel wall, b. corresponding HE image, c. pleuropulmonal blastoma with loss of normal lung architecture and increased cell density in the TPEF signal. Irregular collagen structure and –distribution in the SHG signal, d. corresponding HE image. (For interpretation of the references to color in this figure legend, the reader is referred to the Web version of this article.)

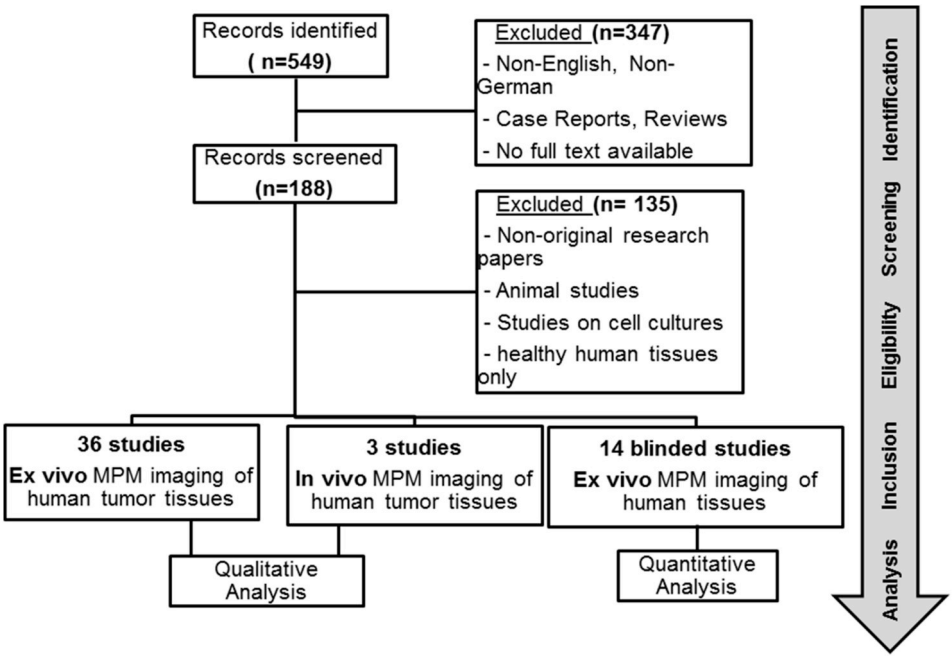

Fig. 5. Preferred Reporting Items for Systematic Reviews and Meta-Analyses (PRISMA) Inclusion flow chart.

four cases, PBS was dripped on the specimens during scanning. When imaging formerly frozen sections, tissue architecture as well as metabolic characteristics [11] can be detected via TPEF/SHG signal. Tissue architecture and extracellular collagen orientation does not seem to be altered by the freezing process [52].

3.2.3. Fixed sections

Only seven studies scanned formalin-fixed or paraffin-embedded tissues [9,12,28,44,47,53,54]. Mehidine et al. compared MPM signals before and after formalin fixation, showing distinct alterations in the TPEF/SHG signal and especially the FILM signal in fixed sections [47]. Other groups showed that TPEF signals may even be enhanced, while SHG and NADH/FAD (necessary to detect the redox ratio) are lost to chemical alteration [53]. However, even after fixation, TPEF signals were found to still be sufficient to detect malignancy [47].

3.2.4. In vivo imaging in human patients

In vivo application of MPM-Imaging in human cancer patients with MPT was described in three studies [6,18,19], in the fields of dermatology [18,19] and neurosurgery [6]. In the dermatological studies, MPT imaging was performed in pigmented suspected malignant skin lesions [18] or suspected basal cell carcinoma in an unsterile setting prior to excision [19]. To minimize motion artefacts, a metal ring was taped to the patients' skin and a magnet on the MPM decreased relative movement of the objective. Kantelhardt et al. described the use of MPT for open brain surgery to determine resection margins in a case of glioblastoma multiforme from the surface of the resection area after durotomy [6]. The instrument was draped sterile and the tip was brought in direct contact to the tissue using a custom-made sterile adaptor and immersion by constant irrigation with normal saline. Images clearly showed loss of tissue architecture typical for high grade malignancy to a tissue depth of 50 μm.

3.3. Detection plane

3.3.1. Tissue sections

Most studies (n = 31) used only perpendicular tissue sections for MPM scanning similar to the sections later fixed and stained with HE. This way, tissue architecture in neighboring sections could be visualized and compared to the gold standard.

3.3.2. Direct visualization through tissue surface

In 18 studies, specimens were scanned directly from the surface in the z-plane without sectioning [5,7,9,16,17,26,31,37,38,43,46,52,55–61]. Fifteen studies used fresh, two frozen [43,52] and one fixed [9] specimen. The specimen was either scanned in a simple glass dish or incubation chamber [31], or was alternatively fixed on the surface with agarose gel [56] or modelling clay [59]. The plane of detection in the z-plane was specified in 10 studies and ranged from 0 μm to 250 μm. This facilitated visualization of esophageal mucosa [55], gastric mucosa [7] or urothelium [37,38] to the level of the lamina propria. A fibrous tumor pseudo capsule [9] or ovary surface epithelium [31] was also penetrated to scan the underlying tissue.

3.4. MPM technology and visualization

3.4.1. Equipment and settings

Most studies were conducted with a conventional commercial MPM microscope combined with a mode-locked femtosecond titanium (Ti): sapphire laser. The mean excitation wavelength (λ_{ex}) was 803 ± 39 nm to produce the TPEF and SHG signals (Fig. 6). Only in one study, two different excitation wavelengths were used for excitation of the TPEF and SHG signal [55]. TPEF emission wavelengths (λ_{em}) was detected at a range of 429 ± 15 nm–668 ± 74 nm, while SHG signal was detected at shorter wavelengths between λ_{em} 384 ± 14 nm and 408 ± 46 nm. For lower magnifications (x4-x24), dry objectives were found to be useable [12,35–38,55], but higher magnifications (>x24-x150) required either water- [55] or oil immersion objectives. In most studies, commercial oil immersion objectives were used.

A commercial MPT-FILM device with integrated tunable Ti:Sappire laser and oil immersion objective was used for the studies in vivo [6,18,19].

3.4.2. Qualitative, examiner-dependent measures

A summary of typical MPM morphological findings for normal tissues und specific tumor entities is given in Table 3.

3.4.2.1. Two-photon excited fluorescence (TPEF). TPEF imaging was

Table 2
Included studies and study characteristics (n.s. = not specified).

Author	Year	Tissue	Number specimens	Tissue preparation
Balu M et al. [18]	2014	skin	15	in vivo
Balu M et al. [19]	2015	skin	10	in vivo
Chen J et al. [74]	2011	gastric wall	20	fresh
Chen J et al. [55]	2014	esophageal mucosa	63	fresh
Chen WS et al. [49]	2014	esophageal mucosa	20	frozen
Chen Y et al. [53]	2014	pancreas	35	fixed
De Giorgi V et al. [56]	2009	skin	n.s.	fresh
Fang N et al. [51]	2019	brain	26	frozen
Goedeke et al. [28]	2019	variuous	7	fixed
Han Z et al. [75]	2019	breast	30	fresh
He K et al. [27]	2018	gastric mucosa	18	fresh
Huang Z et al. [57]	2012	nasopharyngeal mucosa	9	fresh
Huland DM et al. [63]	2014	prostate	14	fresh
Jain M et al. [37]	2012	urothelium	77	fresh
Jain M et al. [35]	2014	lung	50	fresh
Jain M et al. [38]	2015	urothelium	78	fresh
Jain M et al. [36]	2016	kidney	80	fresh
Jain M et al. [12]	2018	kidney	27	fixed
Kantelhardt SR et al. [6]	2016	brain	1	in vivo
Kirkpatrick et al. [31]	2007	ovary	53	fresh
Li L et al. [39]	2014	colorectal mucosa	12	fresh
Li L et al. [76]	2015	rectal wall	7	fresh
Li L et al. [40]	2019	gastric wall	24	frozen
Li LH et al. [41]	2015	colorectal wall	28	fresh
Li X et al. [7]	2018	gastric mucosa	24	fresh
Lin P et al. [54]	2018	brain	34	fixed/fresh
Manfredini M et al. [17]	2013	skin	16	fresh
Mehidine H et al. [47]	2018	brain	46	fresh/fixed
Muensterer et al. [9]	2017	pediatric tumors	7	fixed
Nie YT et al. [64]	2015	breast	12	fresh
Poulon et al. [42]	2018	brain	25	fresh
Qiu J et al. [65]	2015	colorectal submucosa	15	fresh
Rogart et al. [58]	2008	gastrointestinal mucosa	24	fresh
Tewari AK et al. [59]	2010	prostate	95	fresh
Wang CC et al. [50]	2009	lung	10	frozen
Williams RM et al. [25]	2010	ovary	n.s.	fresh
Wu S et al. 1 [11]	2018	breast	23	frozen
Wu S et al. 2 [52]	2018	skin	19	frozen
Wu X et al. [43]	2013	breast	24	frozen
Wu X et al. [26]	2016	breast	60	fresh
Wu Y et al. [77]	2018	breast	12	frozen
Wu Y et al. 1 [78]	2015	breast	19	fresh
Wu Y et al. 2 [79]	2015	breast	40	fresh
Xu J et al. [44]	2013	esophageal mucosa	3	fixed
Xu J et al. 1 [21]	2017	pancreas	8	fresh
Xu J et al. 2 [8]	2017	esophgageal mucosa	34	frozen
Yan J et al. [48]	2011	gastric mucosa	20	frozen
Yan J et al. [45]	2012	liver	224	fresh/frozen
Yan J et al. [16]	2014	rectal mucosa	30	fresh
Ying M et al. [5]	2012	coloractal wall	30	fresh
Yoshitake et al. [61]	2016	breast	179	fresh
Zheng X et al. [46]	2019	gastric wall	70	fresh
Zhou Y et al. [80]	2016	gastric muscular layer	12	fresh

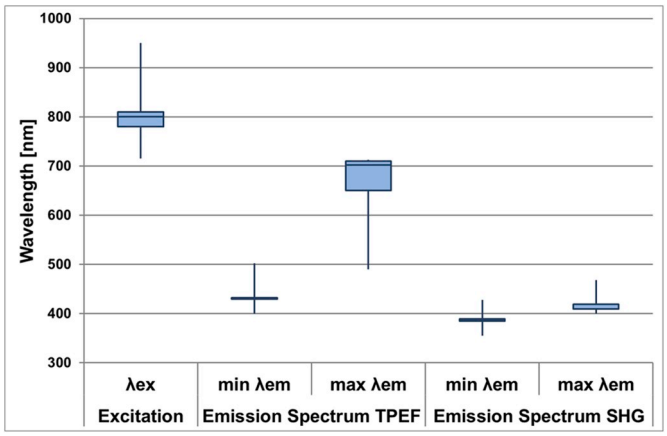

Fig. 6. Boxplot of the excitation wavelengths (λex) and emission spectrum (min λem – max for λem) forTPEF and SHG signal detection used in the included studies. Λex was in the rage of 780–810 nm in 50% of studies. The median detection range was 430–708 nm for TPEF and 387–419 nm for SHG (λ_{ex} = excitation wavelength, λ_{em} = emission wavelength).

performed in all studies. The main signal derives from NADP and FAD of the cytoplasm, mitochondriaor intracellular lipofuscin [12]and granules in mucus cells [62], implying that the TPEF signal is the greatest contributor to visualization of cellular tissue architecture and cell morphology with detail and resolution comparable to HE sections [58]. The nucleus was only detected as an area with absence of TPEF/SHG signal [27,28], which is generally referred to as the "nuclear area". The density of this area increased in deeper tissue layers [57]. Therefore, nuclear margin irregularity, as a sign of cancer cells, was not always easy to objectify in MPM [28], especially in deeper layers [57]. In more superficial layers, however, MPM allowed nuclear margin irregularity [57], or even mitosis, to be visualized by the configuration of the nuclear area [50]. Furthermore, macromolecules such as muscle- [27] and nerve fibers [63], intima of arteries [27], and molecules of the extracellular matrix like elastin, and collagen [12], were visualized with fluorescence peaks at specific excitation wavelengths. In tumors, TPEF signal was usually heightened due to the increased cell density [55], inflammatory cells [7,39] or necrosis [39].

3.4.2.2. Second harmonic generation (SHG). In all but five studies, SHG signal was described. The SHG signal is produced by detection of scattering caused by proteins of the extracellular stroma. In contrast to HE sections, collagen content and orientation was quantifiable [49,64], giving additional information about tumor microenvironment. Collagen type I had both a strong SHG and TPEF signal [27]. Also, basement membranes (containing collagen type IV) were visualized, giving evidence of tumor stage and invasiveness [44]. SHG signal particularly enabled accurate evaluation of the lamina propria, as a sensitive tool to detect early stages of tumor invasion [27,40]. Kirkpatrick et al. were able to show a more linear collagen structure in younger, and a more diffuse collagen structure in older patients' healthy tissues [31]. In

Table 3
Typical morphological findings (TPEF and SHG) for normal tissues und specific tumor entities. (NCR= Nucleus-Cell-Ratio).

	Healthy Tissue			Malignancy criteria	
Tissue origin	TPEF	SHG	Tumor type	TPEF	SHG
adrenal gland	acinar cell architecture	stroma	neuroblastoma	small cells, round nuclei, indistinct cell borders, tumor vessels	
brain	neurons, elastin, lipopigments, porphyrins	collagen, reticulin, blood vessel walls	pituitary hyperplasia	acini longer/more irregular	
			glioblastoma multiforme	disorganized tumorous cell architecture	sparse signal, vascular prolifaration
			brain metastasis	hypercellularity	disorganized stroma
breast	acinus-duct architecture, epithelial cells with bright cytoplasm, fat cells, nucear area	collagen content/-density/-orientation, basement membrane, fine-meshed thick collagen	breast cancer	cellular and nuclear pleomorphism, higher NCR, necrotic cells fill the duct lumen	fragmented collagen fibers, loss of collagen signal, missing basement membrane
			fibrodenoma	compressed ducts	higher collagen content, altered collagen orientation
			fibrocystic lesion	cysts filled with cystic fluid	dense collagen surrounding cysts
colorectal wall	typical foveolar pattern, central/round crypt openings, epithelial cells, goblets cells, submucosal elastic fibers	collagen content and -orientation, submucosa rich in collagen	colorectal carcinoma	irregular tubular structures, pleomorphism, disordered cells, dirty necrosis, lymphocyte infiltration, loss of goblet cells/cellular junctions	reduced stroma, loss of collagen, distorted blood vessels, grading of fibrotic reaction after neo-adjuvant therapy
esophageal wall	keratinocytes, squamous epithelium, blood vessels	lamina propria, submucosa	adenocarcinoma	pleomorph cancerous cells, surrounding fibrous stroma, intestinal metaplasia: columnar epithelium, foveulae, mucous cells, parietal cells, chief cells, lymphozyte infiltration	abscence of basement membrane, disordered and sparser collagen, loss of SHG signal
			intestinal metaplasia	columnar epithelium, foveulae, mucous cells, parietal cells, chief cells, lymphocyte infiltration	
			esophagitis	increased hight of connective tissue papillae, vascular congestion	
gastric wall	cellular architecture	extracellular stroma, honeycomb like collagen structure, submucosa	adenocarcinoma	cell pleomorphims, increased NCR, and necrotic states in the glandular cavity	collagen structure broken by tumor tissue
kidney	glomerulus, tubules, blood vessels, NADH, lipofuscin, collagen type IV	interstitium, collagen, hemosiderin	renal cell carcinoma	large, polygonal cells, distinct cell boarder, inhomogenous cytoplasm, "sandlike" granula,round pleomorphic nuclei, perinuclear halo	
			renal clear cell carcinoma	intracellular fat droplets, low NCR, sheets of tumor cells, thickened blood vessels, intracytoplasmatic granules	
			papillary renal cellcarcinoma	single-layer cuboid cells, papillae with fibro-vascular core, large histiocytes	
			oncocytoma	nested or acinar growth pattern, small cells, homogenous cytoplasm, larger garnulas, regular round signal-void nucleus	
			papillary urothel carcinoma	multi-layered epithelium with fibrovascular core	
			nephroblastoma	unordered tubules, solid atypical tumor cells, stroma with tumor vessels	
liver	radial orientation of hepatocyte cords around central veins and hepatocytes, blood-filled sinusoids	delicate strands of collagen network alongside hepatocytes	hepatocellular carcinoma	cellular and nuclear pleomorphism, increased NCR, thickened trabecular structures, pseudoglandular structures	loss of collagen in the intercellular space
			cholangiocarcinoma	glandular/tubular structures, abundant desmoplastic stromal reaction	dense collagen
			Focal nodular hyperplasia		central collagen and branch
			liver cell adenoma	two-and three-cell-thick liver plates	delicate strands of collagen alongside hepatocytes
			cavernous hemangioma	large, cavernous vascular spaces filled with blood	cavernous collagen structures
			liver cirrhosis	vascular septa rich in elastic fibers	collagenous septa
lung	pneumocytes, lacelike pattern of alveoli (elastin/ collagen), pleura (elastin), lymphocytes, marcorphages	well defined fibrillar architecture of collagen	atypical adenomatous hyperplasia	proliferation of atypical pneumocytes, along the preexisting alveolar wall, discontinuous layer of pneumocytes	
			adenocarcinoma		

(*continued on next page*)

Table 3 (*continued*)

	Healthy Tissue			Malignancy criteria	
Tissue origin	TPEF	SHG	Tumor type	TPEF	SHG
				clear papillary projections composed of cuboidal to columnar cells	collagen-rich fibrovascular cores
			small cell carcinoma	pavementlike malignant cells, complete loss of the normal lung architecture, high NCR	increased collagen content
			squamous cell carcinoma	cellular masses	decreased SHG signal
			pulmonary blastoma	small cells with lack of cytoplasm, round nuclei, cellularity and necrosis	
nasopharyngeal mucosa	honeycomb appearance, cytoplasm, nucelear area		squamous cell carcinoma	cellular pleomorphism, increased NCR	
ovary	cell architecture, single layer squamous surface epithelium, simple cysts near the surface	highly structured collagen in the stroma	ovarian cancer	pleomorph cells forming glandular structure, high NCR	changes in collagen structure, desmoplastic stroma, collagen fibrils perpendicular to invasive edge
pancreas	acinus-duct architecture, boundry of lobule, mucin, basement membrane	concentric fibrous bundles, short and thick collagen fibers, collagen clusters of stroma, basement membrane	pancreatic mucinous neoplasm	single layer columnar, mucin-producing epithelium	dense collagenized stroma
			pancreatic ductal carinoma	irregular glands, necrosis, randomly-arranged endothelium, increased NCR	bands of fibrous stroma, increase of collagen
prostate	acinus-duct architecture, strong punctate autofluorescence in the cytoplasm (lipofuscein), adipocytes, nerve fibers	collagen of the stroma, vas deferens	adenocarcinoma	clusters of small acini, sharp luminal borders, aggregated small secretions in the lumen, loss of architecture	
skin	cell architecture, highly fluorescent cytoplasms and dark nuclei	collagen content/-orientation	basal cell carcinoma	aligned elongated cells, palisading phenomenum, cell islands surrounded by fibers, melanophages, plum bright cells wit ill-defined borders, small cells, reduced fluorescent contrast between cytoplasm and nucleus	
			malignant melanoma	low resolution due to high absorbance of melanin	
			dermatofibrosarcoma	lower collagen intesity, altered cellular structure	alterations in collagen shape, decreased collagen content
urothelium	multilayered urothelium with uniform thickness, umbrella cells, elastin fibers	collagen fibers of the lamina propria	carcinoma in situ	varying surface urothelium, high NCR and marked nuclear pleomorphism, lymphocytes	
			low-grade papillary urothelial carcinoma	papillary fonds with thin, fibrovascular cores, mild pleomorphism, low NCR	
			high-grade papillary urothelial carcinoma	papillary fronds, sheets of tumor cells, moedrate cell and nuclear pleomorphism, high NCR,lLoss of polarity	irregular nests of individual tumor cells und lamina propria or muscularis propria

tumor patients, SHG signal was significantly decreased or lost because of higher cell density [16,43] or heightened in collagen-producing tumors such as cholangiocarcinoma [45] or encapsuled tumors like nephroblastoma [9]. Due to the strong SHG signal in blood vessels, tumor angiogenesis was more clearly visible and earlier detectable in MPM than in HE stained specimen [51]. Changes in collagen content and collagen orientation were able to be assessed objectively by the detection of SHG signal intensity per pixel [11,52,64,65].

3.4.2.3. Detection of malignancy in blinded analysis. In fourteen studies, the MPM examiner was blinded to the gold standard HE result [12,28,35–46]. Studies examined detection of malignancy versus healthy tissues [21,37,38,40,42,43,45], surgical resection margins [21,46], specific tumor entities [12,28,35,36,43] or tumor regression grade after neoadjuvant therapy [41] and dirty necrosis [39] in colorectal carcinoma. In the individual studies, MPM yielded sensitivity of 46–100%, specificity of 35–100%, and accuracy of 61–100%. One study stated the accuracy for detection of dirty necrosis in colorectal carcinoma was 100% [39]. Regarding the detection of neoplasms, imaging of formalin fixed, deparaffinized specimens, yielded comparable sensitivity, specificity and accuracy to fresh or frozen specimen [45].Considering the work of Jain et al. from 2012 to 2018 on urothelium and kidney masses, there seemed to be a considerable learning curve indicated by the improvement of sensitivity, specificity and accuracy over the years, evolving the technique to differentiate between various tumor entities (Table 4). In a subgroup analysis of eight studies (Table 4, *) analyzing the general detection of tumor without further differentiation with a total of 440 samples, MPM had an overall sensitivity 94%, specificity 96% and accuracy of 95% for the detection of malignant tissue (Table 5).

3.4.3. Objective measures in MPM

In addition to subjective, examiner-dependent findings, MPM signals could be analyzed objectively by the computer. Most frequently described objective measures include FILM, optical redox ratio, and automated quantitative detection of the emission spectrum. In some studies, collagen content and –orientation were quantified by automated assessment of the SHG signal, and NCR or TPEF/SHG ratio was analyzed automatically by computer software. Objective, computed measures were found to be specific for each tissue and tumor entity, so that tumor-specific normal values were found that could be employed to interpret the results.

Table 4
Sensitivity, Specificity and Accuracy of blinded studies (RCC = renal cell carcinoma, * included in calculation of detection of malignancy).

Study	tissue	target of visualization	n specimen	n investigartors	sensitivity	specificity	accuracy
Goedeke et al., 2019	various	neuroblastoma	1	38	46	100	61
		rhandomyosarcoma			100	35	66
Jain et al., 2018	kidney	renal oncocytoma in renal masses	27	2	100	100	100
		chromophobe RCC in renal masses			83	100	93
Jain et al., 2016	kidney	clear cell RCC in renal masses	40	2	98	100	99
		papillary RCC in renal masses			95	100	99
		chromophobe RCC in renal masses			80	100	99
		papillary urothelial carcinoma in renal masses			100	100	100
Jain et al., 2015	urothelium	malinancy*	78	2	97	100	99
Jain et al., 2014	lung	lung adenocarcinoma in pulmonal masses	25	2	94	100	96
		lung squamous cell carcinoma in pulmonal masses			57	100	88
Jain et al., 2012	urothelium	malignancy*	77	2	90	77	88
Li L et al., 2019	stomach	malignancy*	24	2	92	100	96
Li LH et al., 2015	colon	tumor regression grade 1	7	1	100	100	100
		tumor regeression grade 2			100	100	100
		tumor regression grade 3			100	100	100
Li L et al., 2014	colon	dirty necrosis	12	1			100
Poulon et al., 2018	brain	malignancy*	25	1	89	71	84
		glioblastoma glioblastoma multiforme			63	80	72
Wu X et al., 2013	breast	fibroadenoma	24	1	100	100	100
		cystic disease			67	94	88
		breast cancer*			100	100	100
Yan J et al., 2012	liver	malignancy*	164	1	96	96	96
Xu et al., 2017 1	pancreas	resection status compared to frozen sections	8	2	100	100	100
		resection status compared to HE sections*				75	75
Zheng X et al., 2019	stomach	clearance of resection margin of gastral tubular adenocarcinoma*	50	2	98	75	94

Table 5
2x2 contingency table after data extraction from eight blinded studies investigating the value of MPM for detection of malignant tissues compared to the gold standard HE sections (n = 440). Overall sensitivity 94%, specificity 96%, accuracy 95%.

	HE goldstandard		
MPM		malignant	benign
	malignant	285	10
	benign	19	252

3.4.3.1. Fluorescence lifetime imaging (FILM). FILM signal is an objective observer-independent measure that was described in seven studies ex vivo [17,42,47,56] and in vivo [6,18,19], showing fluorescence lifetime changes with tumor development even in premalignant lesions [7]. We found available data for glioblastoma multiforme [42,47], and melanoma [56], as well as other skin tumors [17–19]. In highly malignant tumors, such as glioblastoma multiforme or malignant melanoma, FILM curve showed a narrow distribution at longer lifetimes compared to normal tissues [47,56]. The longer fluorescence lifetime was assumed to be an indicator of higher metabolic activity in tumor cells [6]. Given this assumption, unsurprisingly, FILM signal was altered by tissue fixation [47].

3.4.3.2. Optical NADH/FAD redox ratio. The optical redox ratio was calculated in seven studies [11,31,41,42,45,57,60]. The emission peaks (λ_{em}) of NADH (λ_{em} 430–490 nm) and FAD (λ_{em} 500–560 nm) were detected separately to calculate the ORR [66] (ORR = intensity of NADH/intensity of FAD [11]). A correct detection of the ORR depends on optimal settings of detector gain of photomultiplier tube and offset values for the different channels for collecting the NADH and FAD signals [57].The redox ratio in cancer cells was higher compared to healthy tissues, indicating active metabolism [11,31,42,45,60]. In breast and colorectal cancer, the ORR decreased after neoadjuvant treatment of carcinoma in situ, but was still higher than in healthy tissue [11,41]. The ORR may also be used as a marker for tumor progression in colonic cancer, even when scanning for the mucosa surface [60]. The ORR can be calculated in fresh or even frozen specimen [11], after fixation with formalin, the NAD/FAD signal is altered and cannot be used to calculate the ORR [53].

3.5. Critical appraisal of quality and applicability

The selected studies had a consistent design. Most ex vivo imaging studies (n = 50) used one of two similar methods. More than half (n = 26) of studies chose neighboring sections from the same tissue blocks for MPM and HE staining to compare the results, while 19 studies performed the MPM imaging first, with or without prior sectioning, and dyed the same specimens for HE imaging afterwards.

Selection bias is the main concern in the selected studies (Fig. 7a). In 23 reports, specimens of defined diagnosis were chosen consciously, while in 26 studies, the selection process was not elaborated. Further bias was introduced by the fact that in some studies, the same investigator analyzed the MPM and HE image simultaneously (n = 9), or knew the result of the HE investigation by the time of the analysis (n = 14). In 17 studies, it was not stated whether either the MPM or HE examiner had prior knowledge of the outcome of the other test.

Applicability to answer the review question was high in the included studies (Fig. 7b), since the vast majority of the selected studies used very similar study protocols. A small number of studies (n = 3) described only MPM imaging without a gold standard reference. In four studies, only TPEF, but not SHG signal was described. These studies were included in spite of minor differences in the study protocol, because the main investigative questions of the value of MPM imaging for cancer were still addressed.

4. Discussion

MPM technology is based on the two-photon emission theory of 1931 by Nobel Prize winner Maria Goeppert-Mayer [67] and has been adapted for medical use by Denk et al., in 1990 [3]. The groundbreaking work of these two people set the cornerstone for various laser-scanning methods, including reflectance confocal laser microscopy (RCM) [68] or other non-linear scanning technologies based on the application of external fluorophores [61]. Both RCM and MPM can be performed on unlabeled tissues, but MPM penetrates deeper into the tissue while RCM images mainly the surface layer. Therefore, in skin lesions, studies show that image resolution of RCM is sufficient to analyze superficial lesions

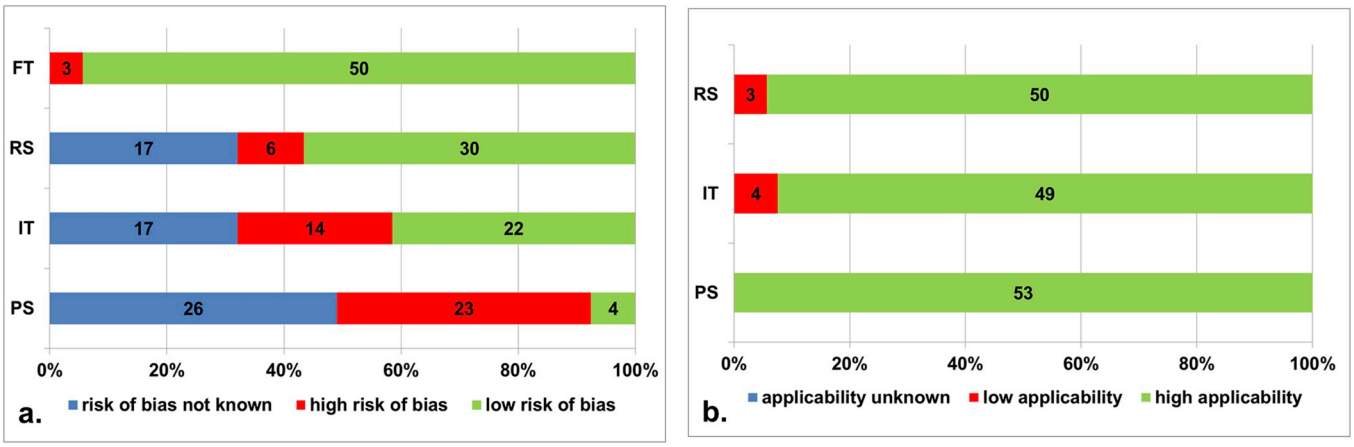

Fig. 7. QUADAS-2 a. Risk of bias, b. Applicability concerns, numbers on the bars refer to the total number of studies in a category, category percentage of included studies is indicated on the y-axis. The rating criteria are shown in the appendix. (FT= Flow and Timing, RS = Reference Standard, IT= Index Test, PS= Patient Selection).

[61]. Also, RCM is much more cost-effective compared to MPM mainly as a result of lower hardware investment costs. However, even though image resolution on the surface seems to be similar [61], in direct comparison MPM offers a higher image resolution in the z-plane, deeper tissue penetrance, and lower phototoxicity [68]. Furthermore, detection of additional MPM signals like second and third harmonic generation provide further valuable diagnostic information [68].

Phototoxicity of MPM imaging is presumed to be low. However, only few studies have actually addressed the subject. Compared to other methods, such as confocal laser microscopy, photobleaching and phototoxicity are more limited to the actual scanning plane with less impact on the surrounding tissue [68]. Débarre et al. showed that there is a cumulative effect of the photon absorption process in *Drosophila* embryos by development of reactive oxygen species (ROS), or even ionization of molecules through laser energy [69]. In their study, phototoxicity could be limited by shifting excitation to longer wavelengths and reducing the repetition rate.

4.1. Advantages and challenges of MPM application in surgical oncology

In basic science research, in vivo MPM imaging has made a major contribution to the understanding of tumor cell behavior. Tumor microenvironment and metabolism [70], signaling pathways [24], tumor migration, progression and metastasing [71], reaction to chemotherapy [72], as well as tumor angiogenesis [73] have been described in a multitude of animal models.

In humans, a CE (Conformité Européenne)-certified device the size of an ultrasound-machine has been developed, and is currently marketed and used for MPT-FILM for in vivo evaluation of skin lesions in the unsterile setting [18,19]. To facilitate transfer to a sterile intraoperative setting in order to evaluate lesions in the operative field or on the body surface, custom-made sterile adapters have to be fashioned and either need to be in direct contact with the region of interest or immersed in an optically inert medium [6]. Even traces of blood can create artefacts during scanning. Furthermore, imaging is influenced by ambient light and is preferably performed in the dark [6].

Systems for optical biopsies through a ridged probe, that can be inserted in a biopsy needle, have been developed [63], but not routinely used. In order to integrate MPM in endoscopes or laparoscopes, much more technical progress is needed, particularly in terms of downsizing the instruments. Furthermore, the necessity of direct contact with the tissue or immersion is an even greater problem, since contamination even with traces of blood or other secretions compromises imaging quality. Subsequently, endoscopic methods using fluid instead of air insufflation, such as cystoscopy, might be a more promising primary target for further investigations than laparoscopy or endoscopy of the gastrointestinal tract. Since scanning fields are extremely small, the region of interest needs to be defined macroscopically with great care before employing in-vivo laser scanning.

For ex vivo use of MPM in patients with suspected cancer, a small number of clinical trials have been published. With the technology available today, instantaneous sections can theoretically be scanned and diagnosed under sterile conditions directly in the operating room after excision by the surgeon, without further sectioning or staining. Image analysis can be supported by artificial intelligence. Since most multiphoton microscopes are sensitive and large devices, they are mostly located in separate laboratories. We expect these instruments to be applicable directly in the operating room with future miniaturization.

4.2. How to use and interpret MPM

In order to achieve high quality imaging and use the full potential of the method, including functional imaging like the optical redox ratio or FILM, fresh tissue samples need be scanned. Best results can be expected by imaging the tissues immediately, but no later than 4 h after excision. This way, FILM and ORR add objective information about the structural and metabolic state of the tissue. The tissue needs to be in direct contact to the lens or immersed in an optically inert fluid. This way, it can be scanned in the z-axis to a depth of several hundred microns from the surface. Definite scanning depth heavily depends on the fluorescence of the tissue. Resolution decreases in deeper scanning planes. Average epithelia can be scanned easily from the tissue surface to the lamina propria, facilitating the diagnosis of carcinoma in situ and early tumor stages, as well as the invasion beyond the lamina propria.

Assessment of normal and atypical cell architecture is possible by the TPEF signal in vivo or in vitro with a comparable resolution to conventional microscopy of HE specimens. The TPEF signal derives from natural fluorophores that are mostly located in the cytoplasm or mitochondria, such as NADH, FAD, but also extracellular molecules like elastin, muscle and nerve fibers [27] or collagen. As a consequence, polymorph tumor cell architecture can be seen in detail. Additionally, relevant structures to define tumor stages like basement membrane [36], the intima of blood vessels or inflammatory cells [41] can be visualized clearly. In microscopic cancer evaluation, many criteria are based on nuclear characteristics. Not being able to visualize the nucleus is one of the major disadvantages of MPM imaging of oncologic tissues. Some information, however, is given by the NCR and configuration of the nuclear area. MPM resolution is high enough to diagnose mitosis by configuration of the nuclear area alone [50].

On the other hand, SHG signal offers the chance to visualize

alterations of the extracellular matrix more accurately than HE staining. Reticulin [54], fibrillar Type I collagen and Type IV collagen, are visualized clearly by the strong TPEF and SHG signal, defining the lamina propria and submucosa. Furthermore, the connective tissue of vessel walls, organ and tumor capsules helps to identify these structures. In malignant tumors, tissue fraction of extracellular matrix is reduced and replaced by polymorph cells. In most tumors, the ratio of TPEF and SHG signal intensity shifts towards TPEF, collagen structure and orientation are altered. By visualizing the basal lamina and lamina propria, carcinoma in situ can be accurately differentiated from invasive tumors.

Additionally, objective measures like FILM, ORR, NCR, collagen content and –orientation can be calculated by the computer in fresh specimens. These data are usually expressed as tables or diagrams, depending on the processing software used. The corresponding values are specific for each tissue, each tumor entity and stage of treatment. To date, normal values exist for only very few tumors. Therefore, further research and the investigation of normal values for each tumor entity are essential.

If MPM is not readily available at all times, frozen, as well as fixed sections yield sufficient TPEF/SHG signal to detect histological signs of malignancy. Possible alterations caused by fixation do not seem to have significant impact on the histological image. Functional imaging, however, is no longer possible.

Our review identified only 14 blinded studies out of a total of 53 included research papers on MPM in cancer patients. After general feasibility has been proved, more blinded studies with larger patient numbers are needed to determine the diagnostic value of the method in terms of sensitivity, specificity and accuracy. For objective measures like FILM, ORR, NCR, collagen content and –orientation, normal values have to be established, using a standard data processing protocol.

5. Conclusion

MPM offers functional real time imaging of human tissues on a microscopic level without tissue preparation in vivo and ex vivo. Imaging can be performed from the tissue surface to a depth of up to 1000 μm, depending on the natural fluorescence of the tissue. Ex vivo, imaging of fresh tissues within an hour after excision offers the best TPEF and SHG signal. In fresh specimen, fluorescence lifetime imaging, virtual histochemistry and optical redox ratio give additional information about the nature and metabolic state of the tissue. Signal intensity per pixel, FILM, ORR and collagen content, as well as three-dimensional distribution patterns can be objectively detected by the computer independent of the observer.

Images of general and MPM specific tumor characteristics can be obtained with high accuracy, even though standard pathology in tumors is highly dependent on nuclear characteristics, which cannot be visualized by MPM directly. Instead, other tumor characteristics, such as alterations in the connective tissue, are easier to detect and can be measured objectively.

MPT-FILM is already used for in vivo three-dimensional tissue evaluation in dermatology in an unsterile setting, and in one case in the sterile setting of neurosurgery. Further significant technical advances are needed to incorporate the technology into the fields of endoscopy and minimally invasive surgery.

In summary, MPM is a promising relatively new technology that has been proven to be useful in the intraoperative diagnosis of neoplasms and is at the point of attaining clinical applicability in the near future by further miniaturization, standardization, and the combination with artificial intelligence.

Contributions

The study was planned by TTK. TTK and JG individually selected papers to be included in the review and performed the analysis of risk of bias and applicability. The process was supervised by OJM. TTK and OJM contributed to writing the final version of the manuscript.

Funding

This research did not receive any specific grant from funding agencies in the public, commercial, or not-for-profit sectors.

Key points

- MPM offers functional real time imaging of human tissues on a microscopic level without tissue preparation in vivo or ex vivo.
- Ex vivo, imaging of fresh tissues within an hour after excision offers the best TPEF and SHG signal and additional objective functional imaging.
- With MPM, tumor cells can be detected with a high sensitivity and specificity, even though the cell nucleus cannot be visualized.
- Use of MPM in a sterile field of open surgery is feasible but requires extensive preparation.
- In order to incorporate the technology in endoscopic procedures, technical innovation is mandatory.

Declaration of competing interest

None.

Acknowledgements

The authors wish to offer special thanks to Dr. Larissa Seidmann of our Department of Pathology for contribution of corresponding HE images.

Appendix A. Supplementary data

Supplementary data to this article can be found online at https://doi.org/10.1016/j.suronc.2019.10.011.

Appendix

Search Strategy

(("multiphoton microscopy" OR "multi-photon microscopy" OR "multi photon microscopy" OR "multiphoton fluorescence microscopy" OR "multi-photon fluorescence microscopy" OR "multi photon fluorescence microscopy" OR "two-photon microscopy" OR "two photon microscopy" OR "two-photon excitation microscopy" OR "two photon excitation microscopy")) AND (cancer OR oncol* OR neoplasm* OR tumor OR carcinom* OR sarcom*)

QUADAS-2 Questions for quality and accuracy assessment(34)

Risk of bias

Patient selection: Random or consecutive sample? Inappropriate exclusions?

Index test: Did the MPM investigator know the result of standard histology?

Are there concerns about the qualification of the investigator?

Reference standard: Did the investigator of standard histology know the MPM result?

Are there concerns about the qualification of the investigator?

Flow and Timing: Did all patients receive standard histology?

Were all samples included in the analysis?

Applicability concerns

Sample selection: Human malignant or benignant tumor tissue?

Index test: Did the study investigate both TPEF and SHG signals?

Reference standard: Did the study compare to standard histology?

References

[1] K.W. Dunn, T.A. Sutton, Functional studies in living animals using multiphoton microscopy, ILAR J. 49 (1) (2008) 66–77.

[2] W. Wu, J. Lin, S. Wang, Y. Li, M. Liu, G. Liu, et al., A novel multiphoton microscopy images segmentation method based on superpixel and watershed, J. Biophot. 10 (4) (2017) 532–541.

[3] W.S.J. Denk, W.W. Webb, Two-photon laser scanning fluorescence microscopy, Science 248 (1990) 73–76.

[4] A. Li, G. Hall, D. Chen, W. Liang, B. Ning, H. Guan, et al., A biopsy-needle compatible varifocal multiphoton rigid probe for depth-resolved optical biopsy, J. Biophot. 12 (1) (2019), https://doi.org/10.1002/jbio.201800229 e201800229.

[5] M. Ying, S. Zhuo, G. Chen, C. Zhuo, J. Lu, W. Zhu, et al., Real-time noninvasive optical diagnosis for colorectal cancer using multiphoton microscopy, Scanning 34 (3) (2012) 181–185.

[6] S.R. Kantelhardt, D. Kalasauskas, K. Konig, E. Kim, M. Weinigel, A. Uchugonova, et al., In vivo multiphoton tomography and fluorescence lifetime imaging of human brain tumor tissue, J. Neuro Oncol. 127 (3) (2016) 473–482.

[7] X. Li, H. Li, X. He, T. Chen, X. Xia, C. Yang, et al., Spectrum- and time-resolved endogenous multiphoton signals reveal quantitative differentiation of premalignant and malignant gastric mucosa, Biomed. Opt. Express 9 (2) (2018) 453–471.

[8] J. Xu, D. Kang, Y. Zeng, S. Zhuo, X. Zhu, L. Jiang, et al., Multiphoton microscopy for label-free identification of intramural metastasis in human esophageal squamous cell carcinoma, Biomed. Opt. Express 8 (7) (2017) 3360–3368.

[9] O.J. Muensterer, S. Waldron, Y.J. Boo, C. Ries, L. Sehls, F. Simon, et al., Multiphoton microscopy: a novel diagnostic method for solid tumors in a prospective pediatric oncologic cohort, an experimental study, Int. J. Surg. 48 (2017) 128–133.

[10] M.J. Huttunen, A. Hassan, C.W. McCloskey, S. Fasih, J. Upham, B.C. Vanderhyden, et al., Automated classification of multiphoton microscopy images of ovarian tissue using deep learning, J. Biomed. Opt. 23 (6) (2018) 1–7.

[11] S. Wu, Y. Huang, Q. Tang, Z. Li, H. Horng, J. Li, et al., Quantitative evaluation of redox ratio and collagen characteristics during breast cancer chemotherapy using two-photon intrinsic imaging, Biomed. Opt. Express 9 (3) (2018) 1375–1388.

[12] M. Jain, B.D. Robinson, B. Wu, F. Khani, S. Mukherjee, Exploring multiphoton microscopy as a novel tool to differentiate chromophobe renal cell carcinoma from oncocytoma in fixed tissue sections, Arch. Pathol. Lab Med. 142 (3) (2018) 383–390.

[13] T.Y. Sun, A.M. Haberman, V. Greco, Preclinical advances with multiphoton microscopy in live imaging of skin cancers, J. Investig. Dermatol. 137 (2) (2017) 282–287.

[14] H. Tu, Y. Liu, D. Turchinovich, M. Marjanovic, J. Lyngso, J. Laegsgaard, et al., Stain-free histopathology by programmable supercontinuum pulses, Nat. Photonics 10 (8) (2016) 534–540.

[15] K. Konig, Multiphoton microscopy in life sciences, J. Microsc. 200 (Pt 2) (2000) 83–104.

[16] J. Yan, S. Zhuo, G. Chen, J.W. Milsom, H. Zhang, J. Lu, et al., Real-time optical diagnosis for surgical margin in low rectal cancer using multiphoton microscopy, Surg. Endosc. 28 (1) (2014) 36–41.

[17] M. Manfredini, F. Arginelli, C. Dunsby, P. French, C. Talbot, K. Konig, et al., High-resolution imaging of basal cell carcinoma: a comparison between multiphoton microscopy with fluorescence lifetime imaging and reflectance confocal microscopy. Skin research and technology, Off.J. Int. Soc. Bioeng. Skin(ISBS).Int. Soc. Digit. Imag. Skin(ISDIS). Int. Soc. Skin. Imag 19 (1) (2013) e433–e443.

[18] M. Balu, K.M. Kelly, C.B. Zachary, R.M. Harris, T.B. Krasieva, K. Konig, et al., Distinguishing between benign and malignant melanocytic nevi by in vivo multiphoton microscopy, Cancer Res. 74 (10) (2014) 2688–2697.

[19] M. Balu, C.B. Zachary, R.M. Harris, T.B. Krasieva, K. Konig, B.J. Tromberg, et al., In vivo multiphoton microscopy of basal cell carcinoma, JAMA dermatology 151 (10) (2015) 1068–1074.

[20] B.W. Graf, S.A. Boppart, Multimodal in vivo skin imaging with integrated optical coherence and multiphoton microscopy, IEEE J. Sel. Top. Quantum Electron. : Publication.IEEE. Lasers.Electro-Optics Soc. 18 (4) (2012) 1280–1286.

[21] J. Xu, Y. Chen, H. Chen, Z. Hong, Z. Shi, S. Zhuo, et al., Identifying the neck margin status of ductal adenocarcinoma in the pancreatic head by multiphoton microscopy, Sci. Rep. 7 (1) (2017) 4586.

[22] M. Durand, M. Jain, A. Aggarwal, B.D. Robinson, A. Srivastava, R. Smith, et al., Real-time in vivo periprostatic nerve tracking using multiphoton microscopy in a rat survival surgery model: a promising pre-clinical study for enhanced nerve-sparing surgery, BJU Int. 116 (3) (2015) 478–486.

[23] H. Lin, C. Wei, G. Wang, H. Chen, L. Lin, M. Ni, et al., Automated classification of hepatocellular carcinoma differentiation using multiphoton microscopy and deep learning, J. Biophot. 12 (7) (2019), https://doi.org/10.1002/jbio.201800435 e201800435.

[24] T. Imamura, T. Saitou, R. Kawakami, In vivo optical imaging of cancer cell function and tumor microenvironment, Cancer Sci. 109 (4) (2018) 912–918.

[25] R.M. Williams, A. Flesken-Nikitin, L.H. Ellenson, D.C. Connolly, T.C. Hamilton, A. Y. Nikitin, et al., Strategies for high-resolution imaging of epithelial ovarian cancer by laparoscopic nonlinear microscopy, Transl. Oncol. 3 (3) (2010) 181–194.

[26] X. Wu, G. Chen, J. Qiu, J. Lu, W. Zhu, J. Chen, et al., Visualization of basement membranes in normal breast and breast cancer tissues using multiphoton microscopy, Oncology letters 11 (6) (2016) 3785–3789.

[27] K. He, L. Zhao, X. Huang, Y. Ding, L. Liu, X. Wang, et al., Label-free imaging for T staging of gastric carcinoma by multiphoton microscopy, Lasers Med. Sci. 33 (4) (2018) 871–882.

[28] J.S.P. Goedeke, L. Seidmann, G. Li, J. Birkenstock, F. Simon, J. König, O. J. Muensterer, Multiphoton microscopy in the diagnostic assessment of pediatric solid tissue in comparison to conventional histopathology: results of the first international online interobserver trial, Cancer Manag. Res. (11) (2019) 3655–3667.

[29] C. Su Lim, E. Sun Kim, J. Yeon Kim, S. Taek Hong, H. Jai Chun, D. Eun Kang, et al., Measurement of the nucleus area and nucleus/cytoplasm and mitochondria/nucleus ratios in human colon tissues by dual-colour two-photon microscopy imaging, Sci. Rep. 5 (2015) 18521.

[30] S. Desir, P. O'Hare, R.I. Vogel, W. Sperduto, A. Sarkari, E.L. Dickson, et al., Chemotherapy-induced tunneling nanotubes mediate intercellular drug efflux in pancreatic cancer, Sci. Rep. 8 (1) (2018) 9484.

[31] N.D. Kirkpatrick, M.A. Brewer, U. Utzinger, Endogenous optical biomarkers of ovarian cancer evaluated with multiphoton microscopy. Cancer epidemiology, biomarkers & prevention : a publication of the American Association for Cancer Research, Cosponsored.Am. Soc. Prev.Oncol. 16 (10) (2007) 2048–2057.

[32] M. Lee, A. Serrels, Multiphoton microscopy for visualizing lipids in tissue, Methods Mol. Biol. 1467 (2016) 105–118.

[33] T. Wang, D.G. Ouzounov, C. Wu, N.G. Horton, B. Zhang, C.H. Wu, et al., Three-photon imaging of mouse brain structure and function through the intact skull, Nat. Methods 15 (10) (2018) 789–792.

[34] P.F. Whiting, A.W. Rutjes, M.E. Westwood, S. Mallett, J.J. Deeks, J.B. Reitsma, et al., QUADAS-2: a revised tool for the quality assessment of diagnostic accuracy studies, Ann. Intern. Med. 155 (8) (2011) 529–536.

[35] M. Jain, N. Narula, A. Aggarwal, B. Stiles, M.M. Shevchuk, J. Sterling, et al., Multiphoton microscopy: a potential "optical biopsy" tool for real-time evaluation of lung tumors without the need for exogenous contrast agents, Arch. Pathol. Lab Med. 138 (8) (2014) 1037–1047.

[36] M. Jain, B.D. Robinson, A. Aggarwal, M.M. Shevchuk, D.S. Scherr, S. Mukherjee, Multiphoton microscopy for rapid histopathological evaluation of kidney tumours, BJU Int. 118 (1) (2016) 118–126.

[37] M. Jain, B.D. Robinson, D.S. Scherr, J. Sterling, M.M. Lee, J. Wysock, et al., Multiphoton microscopy in the evaluation of human bladder biopsies, Arch. Pathol. Lab Med. 136 (5) (2012) 517–526.

[38] M. Jain, B.D. Robinson, M.M. Shevchuk, A. Aggarwal, B. Salamoon, J.M. Dubin, et al., Multiphoton microscopy: a potential intraoperative tool for the detection of carcinoma in situ in human bladder, Arch. Pathol. Lab Med. 139 (6) (2015) 796–804.

[39] L. Li, W. Jiang, Y. Yang, Z. Chen, C. Feng, H. Li, et al., Identification of dirty necrosis in colorectal carcinoma based on multiphoton microscopy, J. Biomed. Opt. 19 (6) (2014), 066008.

[40] L. Li, D. Kang, Z. Huang, Z. Zhan, C. Feng, Y. Zhou, et al., Multimodal multiphoton imaging for label-free monitoring of early gastric cancer, BMC Canc. 19 (1) (2019) 295.

[41] L.H. Li, Z.F. Chen, X.F. Wang, S.M. Zhuo, H.S. Li, W.Z. Jiang, et al., Multiphoton microscopy for tumor regression grading after neoadjuvant treatment for colorectal carcinoma, World J. Gastroenterol. 21 (14) (2015) 4210–4215.

[42] F. Poulon, J. Pallud, P. Varlet, M. Zanello, F. Chretien, E. Dezamis, et al., Real-time Brain Tumor imaging with endogenous fluorophores: a diagnosis proof-of-concept study on fresh human samples, Sci. Rep. 8 (1) (2018) 14888.

[43] X. Wu, G. Chen, J. Lu, W. Zhu, J. Qiu, J. Chen, et al., Label-free detection of breast masses using multiphoton microscopy, PLoS One 8 (6) (2013), e65933.

[44] J. Xu, D. Kang, M. Xu, S. Zhuo, X. Zhu, J. Chen, Multiphoton microscopic imaging of esophagus during the early phase of tumor progression, Scanning 35 (6) (2013) 387–391.

[45] J. Yan, S. Zhuo, G. Chen, X. Wu, D. Zhou, S. Xie, et al., Preclinical study of using multiphoton microscopy to diagnose liver cancer and differentiate benign and malignant liver lesions, J. Biomed. Opt. 17 (2) (2012), 026004.

[46] X. Zheng, N. Zuo, H. Lin, L. Zheng, M. Ni, G. Wu, et al., Margin diagnosis for endoscopic submucosal dissection of early gastric cancer using multiphoton microscopy, Surg. Endosc. (2019), https://doi.org/10.1007/s00464-019-06783-1.

[47] H. Mehidine, M. Sibai, F. Poulon, J. Pallud, P. Varlet, M. Zanello, et al., Multimodal imaging to explore endogenous fluorescence of fresh and fixed human healthy and tumor brain tissues, J. Biophot. 12 (3) (2019), https://doi.org/10.1002/jbio.201800178 e201800178.

[48] J. Yan, G. Chen, J. Chen, N. Liu, S. Zhuo, H. Yu, et al., A pilot study of using multiphoton microscopy to diagnose gastric cancer, Surg. Endosc. 25 (5) (2011) 1425–1430.

[49] W.S. Chen, Y. Wang, N.R. Liu, J.X. Zhang, R. Chen, Multiphoton microscopic imaging of human normal and cancerous oesophagus tissue, J. Microsc. 253 (1) (2014) 79–82.

[50] C.C. Wang, F.C. Li, R.J. Wu, V.A. Hovhannisyan, W.C. Lin, S.J. Lin, et al., Differentiation of normal and cancerous lung tissues by multiphoton imaging, J. Biomed. Opt. 14 (4) (2009), 044034.

[51] N. Fang, Z. Wu, X. Wang, D. Kang, L. Li, Y. Chen, et al., Automatic and label-free identification of blood vessels in gliomas using the combination of multiphoton microscopy and image analysis, J. Biophot. 12 (9) (2019), https://doi.org/10.1002/jbio.201900006 e201900006.

[52] S. Wu, Y. Huang, Z. Li, H. Wu, H. Li, Collagen features of dermatofibrosarcoma protuberans skin base on multiphoton microscopy, Technol. Cancer Res. Treat. 17 (2018), 1533033818796775.

[53] Y. Chen, J. Chen, H. Chen, Z. Hong, X. Zhu, S. Zhuo, et al., Multiphoton microscopy as a diagnostic imaging modality for pancreatic neoplasms without hematoxylin and eosin stains, J. Biomed. Opt. 19 (9) (2014) 96008.

[54] P. Lin, X. Liu, S. Wang, X. Li, Y. Song, L. Li, et al., Diagnosing pituitary adenoma in unstained sections based on multiphoton microscopy, Pituitary 21 (4) (2018) 362–370.
[55] J. Chen, S. Wong, M.H. Nathanson, D. Jain, Evaluation of Barrett esophagus by multiphoton microscopy, Arch. Pathol. Lab Med. 138 (2) (2014) 204–212.
[56] V. De Giorgi, D. Massi, S. Sestini, R. Cicchi, F.S. Pavone, T. Lotti, Combined non-linear laser imaging (two-photon excitation fluorescence microscopy, fluorescence lifetime imaging microscopy, multispectral multiphoton microscopy) in cutaneous tumours: first experiences, J. Eur. Acad. Dermatol. Venereol. : JEADV 23 (3) (2009) 314–316.
[57] Z. Huang, J. Pan, G. Chen, Z. Li, X. Chen, Y. Li, et al., Fractal analysis of two-photon microscopic images for diagnosis of nasopharyngeal cancer, Scanning 34 (6) (2012) 399–403.
[58] J.N. Rogart, J. Nagata, C.S. Loeser, R.D. Roorda, H. Aslanian, M.E. Robert, et al., Multiphoton imaging can be used for microscopic examination of intact human gastrointestinal mucosa ex vivo, Clin. Gastroenterol. Hepatol. : Off. Clin.Pract. J. Am.Gastroenterol.Assoc. 6 (1) (2008) 95–101.
[59] A.K. Tewari, M.M. Shevchuk, J. Sterling, S. Grover, M. Herman, R. Yadav, et al., Multiphoton microscopy for structure identification in human prostate and periprostatic tissue: implications in prostate cancer surgery, BJU Int. 108 (9) (2011) 1421–1429.
[60] S. Zhuo, J. Yan, G. Chen, J. Chen, Y. Liu, J. Lu, et al., Label-free monitoring of colonic cancer progression using multiphoton microscopy, Biomed. Opt. Express 2 (3) (2011) 615–619.
[61] T. Yoshitake, M.G. Giacomelli, L.C. Cahill, D.B. Schmolze, H. Vardeh, B. E. Faulkner-Jones, et al., Direct comparison between confocal and multiphoton microscopy for rapid histopathological evaluation of unfixed human breast tissue, J. Biomed. Opt. 21 (12) (2016) 126021.
[62] N. Liu, G. Chen, J. Chen, J. Yan, S. Zhuo, L. Zheng, et al., Multiphoton microscopic imaging of normal human rectum tissue, Scanning 32 (6) (2010) 347–350.
[63] D.M. Huland, M. Jain, D.G. Ouzounov, B.D. Robinson, D.S. Harya, M.M. Shevchuk, et al., Multiphoton gradient index endoscopy for evaluation of diseased human prostatic tissue ex vivo, J. Biomed. Opt. 19 (11) (2014) 116011.
[64] Y.T. Nie, Y. Wu, F.M. Fu, Y.E. Lian, S.M. Zhuo, C. Wang, et al., Differentiating the two main histologic categories of fibroadenoma tissue from normal breast tissue by using multiphoton microscopy, J. Microsc. 258 (1) (2015) 79–85.
[65] J. Qiu, W. Jiang, Y. Yang, C. Feng, Z. Chen, G. Guan, et al., Monitoring changes of tumor microenvironment in colorectal submucosa using multiphoton microscopy, Scanning 37 (1) (2015) 17–22.
[66] Z.N. Zhou, P.J. Boimel, J.E. Segall, Tumor-stroma: in vivo assays and intravital imaging to study cell migration and metastasis, Drug Discov. Today Dis. Model. 8 (2–3) (2011) 95–112.
[67] A. Grzybowski, K. Pietrzak, Maria Goeppert-Mayer (1906-1972): two-photon effect on dermatology, Clin. Dermatol. 31 (2) (2013) 221–225.
[68] P. Obeidy, P.L. Tong, W. Weninger, Research techniques made simple: two-photon intravital imaging of the skin, J. Investig. Dermatol. 138 (4) (2018) 720–725.
[69] D. Debarre, N. Olivier, W. Supatto, E. Beaurepaire, Mitigating phototoxicity during multiphoton microscopy of live Drosophila embryos in the 1.0-1.2 microm wavelength range, PLoS One 9 (8) (2014), e104250.
[70] T.M. Heaster, A.J. Walsh, Y. Zhao, S.W. Hiebert, M.C. Skala, Autofluorescence imaging identifies tumor cell-cycle status on a single-cell level, J. Biophot. 11 (1) (2018).
[71] K. Tanaka, Y. Toiyama, Y. Okugawa, M. Okigami, Y. Inoue, K. Uchida, et al., In vivo optical imaging of cancer metastasis using multiphoton microscopy: a short review, Am. J. Tourism Res. 6 (3) (2014) 179–187.
[72] K. Tanaka, M. Okigami, Y. Toiyama, Y. Morimoto, K. Matsushita, M. Kawamura, et al., In vivo real-time imaging of chemotherapy response on the liver metastatic tumor microenvironment using multiphoton microscopy, Oncol. Rep. 28 (5) (2012) 1822–1830.
[73] G.M. Tozer, S.M. Ameer-Beg, J. Baker, P.R. Barber, S.A. Hill, R.J. Hodgkiss, et al., Intravital imaging of tumour vascular networks using multi-photon fluorescence microscopy, Adv. Drug Deliv. Rev. 57 (1) (2005) 135–152.
[74] J. Chen, S. Zhuo, G. Chen, J. Yan, H. Yang, N. Liu, et al., Establishing diagnostic features for identifying the mucosa and submucosa of normal and cancerous gastric tissues by multiphoton microscopy, Gastrointest. Endosc. 73 (4) (2011) 802–807.
[75] Z. Han, L. Li, D. Kang, Z. Zhan, H. Tu, C. Wang, et al., Label-free detection of residual breast cancer after neoadjuvant chemotherapy using biomedical multiphoton microscopy, Lasers Med. Sci. 34 (8) (2019) 1595–1601.
[76] L. Li, Z. Chen, X. Wang, H. Li, W. Jiang, S. Zhuo, et al., Detection of morphologic alterations in rectal carcinoma following preoperative radiochemotherapy based on multiphoton microscopy imaging, BMC Canc. 15 (2015) 142.
[77] Y. Wu, Y. Lin, Y. Lian, P. Lin, S. Wang, F. Fu, et al., Identifying two common types of breast benign diseases based on multiphoton microscopy, Scanning 2018 (2018) 3697063.
[78] Y. Wu, F. Fu, Y. Lian, J. Chen, C. Wang, Y. Nie, et al., Monitoring morphological alterations during invasive ductal breast carcinoma progression using multiphoton microscopy, Lasers Med. Sci. 30 (3) (2015) 1109–1115.
[79] Y. Wu, F. Fu, Y. Lian, Y. Nie, S. Zhuo, C. Wang, et al., Monitoring the progression from intraductal carcinoma to invasive ductal carcinoma based on multiphoton microscopy, J. Biomed. Opt. 20 (9) (2015), 096007.
[80] Y. Zhou, D. Kang, Z. Yang, L. Li, S. Zhuo, X. Zhu, et al., Imaging normal and cancerous human gastric muscular layer in transverse and longitudinal sections by multiphoton microscopy, Scanning 38 (4) (2016) 357–364.
[81] K. Tilbury, P.J. Campagnola, Applications of second-harmonic generation imaging microscopy in ovarian and breast cancer, Perspect. Med. Chem. 7 (2015) 21–32.
[82] M. Kaatz, K. Konig, [Multiphoton microscopy and in vivo tomography in dermatologic imaging]. Der Hautarzt; Zeitschrift Fur Dermatologie, Venerologie, und verwandte Gebiete 61 (5) (2010) 397–409.